Nanoscale

Stabilizing the commensurate charge-density wave in 1T-Tantalum Disulfide at higher temperatures via Potassium Intercalation

Journal:	*Nanoscale*
Manuscript ID	NR-ART-12-2018-009732.R1
Article Type:	Paper
Date Submitted by the Author:	25-Feb-2019
Complete List of Authors:	Zhao, Rui; Pennsylvania State University, Materials Science and Engineering Grisafe, Benjamin; University of Notre Dame Ghosh, Ram Krishna ; University of Notre Dame Wang, Ke; Pennsylvania State University Datta, Suman; University of Notre Dame Robinson, J; Pennsylvania State University, Materials Science and Engineering

Stabilizing the *commensurate* charge-density wave in 1T-Tantalum Disulfide at higher temperatures via Potassium Intercalation

Rui Zhao[1,2], Benjamin Grisafe[3], Ram Krishna Ghosh[3,4], Ke Wang[5], Suman Datta[3], Joshua Robinson[1,2*]

[1] Department of Materials Science and Engineering, The Pennsylvania State University, University Park, PA, 16802, USA
[2] The Center for 2-Dimensional and Layered Materials, The Pennsylvania State University, University Park, PA, 16802, USA
[3] Department of Electrical Engineering, University of Notre Dame, Notre Dame, IN, 46556, USA
[4] Special Centre for Nanoscience, Jawaharlal Nehru University, New Delhi 110067, India
[5] Materials Research Institute, The Pennsylvania State University, University Park, PA, 16802, USA
Corresponding author: * email: jrobinson@psu.edu

Abstract

The 1T phase of Tantalum Disulfide (1T-TaS_2) possesses a variety of charge-density-wave (CDW) orders, and as a result, attracts an increasing amount of academic and technological interests. Researchers have devoted tremendous efforts in understanding the impacts of doping, alloying, intercalation or other triggering agents on its charge density wave orders. In this work, we demonstrate that incorporating potassium chloride (KCl) during chemical vapor deposition (CVD) of TaS_2 can control the phase (1T, 2H or metal nanowire) via intercalation of potassium ions (K^+) between TaS_2 layers. Finally, we demonstrate that K^+ not only impacts the structure during synthesis, but also strongly impacts the CDW phase transition as a function of temperature, increasing the nearly commensurate (NCCDW) to commensurate (CCDW) transition to just below room temperature.

Introduction

Two-dimensional (2D) transition metal dichalcogenides (TMDs) exhibit properties that may have an impact on scientific research and technological applications[1–4]. Exhibiting an extra non-bonding d-orbital electron, the group-V TMDs present metallic properties. As a result of electron-electron and electron-phonon correlations, these materials are prone to reflect a series of quantum physical behaviors, such as superconductivity, magnetism, and charge-density-waves (CDW)[5]. Specifically, TaS_2 has been studied for decades due to the richness and complexity in its charge-density-wave phases and presence of superconductivity[6]. Specifically, the 1T phase of TaS_2 undergoes several phase transitions in which both charge and structural distortions occur. Pristine 1T-TaS_2 transforms from an undistorted high-temperature phase to incommensurate CDW (ICCDW) at 550K; to near-commensurate CDW (NCCDW) at 350K; and finally reaches commensurate CDW (CCDW) at 180K[7]. Through the NCCDW-to-CCDW phase transition, lattice

distortions along with charge redistribution drives a Mott-Hubbert metal-insulator transition (MIT), which leads to a strong modification in electrical properties[7–9]. These phase transitions are also strongly dependent on thickness[10] or external factors such as doping[11], alloying[12], intercalation[13], ambient pressure[14], substrate strain[15], electric field[10,16] or photon impingement[17]. Recent work has been devoted to benchmark ultra-low power devices by integrating 1T-TaS_2 with other materials to make devices such as a 2D phase FET based on 1T-TaS_2 and MoS_2[18], a charge-density-wave oscillator[19], and 1T-TaS_2 memristors[20], to name a few. To date, such reports often utilize high quality single crystal 1T-TaS_2 from chemical vapor transport (CVT)[21], with measurements being carried out at low temperatures[22]. To enhance synthesis scalability, and reduce contamination and oxidation risks from exfoliation process, chemical vapor deposition (CVD) remains an attractive route[23]. Tantalum chloride ($TaCl_5$) and hydrogen sulfide (H_2S) has been utilized as precursors for CVD synthesis and demonstration of robust charge density waves in the as-synthesized flakes[24,25]. However, extra efforts must be devoted when dealing with H_2S to circumvent safety concerns. Previously, we designed a tellurium (Te)-assisted, solid source CVD route to synthesize 1T-TaS_2 crystals using safer chemicals (99.99% tantalum-Ta powder and 99.99% sulfur-S flakes)[26]. Here, we demonstrate that by adding "salt" - potassium chloride (KCl) - during the synthesis, the growth coverage increases by 6-8 times, and K-intercalation in 1T-TaS_2 can induce modifications to the NCCDW-to-CCDW phase transition temperature. Finally, we demonstrate that interlayer K^+ within 1T-TaS_2 flakes can help stabilize the technologically important CCDW phase near room temperature. Supporting density function theory (DFT) calculation verifies that the crystal binding energy is the lowest when K^+ interlayers are added between TaS_2 layers.

Results and discussion

Most inorganic tantalum precursors are chemically stable and difficult to directly sulfurize[27,28]. We previously demonstrated Te-assisted growth[26]; however, due to the low vapor pressure of a Ta-Te or TaS_2 (precursor)-Te mixture, the growth deposition rate and film coverage is limited (~20-30% coverage). Thus, it is worth exploring other additives to synthesize TaS_2. There have been many reports emphasizing the important role that alkali chlorides have played in 2D material synthesis by improving single crystal domain size and promoting lateral growth[29,30]. Here, we choose one particular salt- potassium chloride (KCl). Since low deposition temperatures favor 2H-TaS_2 formation[31], growth additives' lattice energy should not be too low (promotes 2H-TaS_2 formation) or too high (limits evaporation/deposition rates). Among the commercially available salt chemicals (KI, KCl and NaCl), KCl is expected to be the most proper candidate since its melting point is lower than that of NaCl while falling in the temperature range[32] where 1T-TaS_2 is more thermal-dynamically favorable[33]. On the other side, KI's melting point favors 2H growth[32]. The synthesis is carried out in a tube furnace (Figure 1a) with KCl and TaS_2 mixed powders. Experiment details can be found in Supplement information (SI). The KCl not only helps increase deposition coverage by 6-8 times, but also dominates the phase of the as-synthesized flakes. As summarized in Figure 1c, when increasing the amount of KCl at a fixed deposition temperature (850^0C), the deposited 2D layers change from 1T to 2H phase, and finally are converted to quasi 1D Ta nanowires. This

is because with higher amount of potassium ions terminating substrate surface's dangling bonds, atoms' mobility is greatly enhanced, thus the crystal formation energy is lowered[29]. When KCl ratio is increased during the synthesis, more deposition would occur at lower temperatures[34] which thermodynamically favors 2H-TaS_2 formation[33] or even Ta nanowires. The latter case indicates that the bonding between K^+ and S^{2-} is another crucial factor to be considered during this KCl-enhanced growth. Within the $TaS_{2\ precursor}$: KCl ratio range of 6-7 (orange dot in Figure 1c), the flake morphology (Figure 1b) is strikingly different than triangle or hexagon, which are conventional shapes of 2D TMD crystals. Based on energy-dispersive x-ray spectroscopy (Figure S2), a non-negligible K signal is present in the TaS_2 region. This suggests that potassium ions may be incorporated into the 1T-TaS_2 flakes. Therefore, we hypothesize that at elevated temperature, KCl dissociates into potassium ions and chloride ions and catalyzes the vaporization of the TaS_2 precursor powder. Excess potassium ions deposit on the substrate surface, terminating dangling bonds and promoting lateral growth of TaS_2 single crystal. At optimal ratios between TaS_2: KCl, K^+ are incorporated into TaS_2 flakes while 1T phase remains secured.

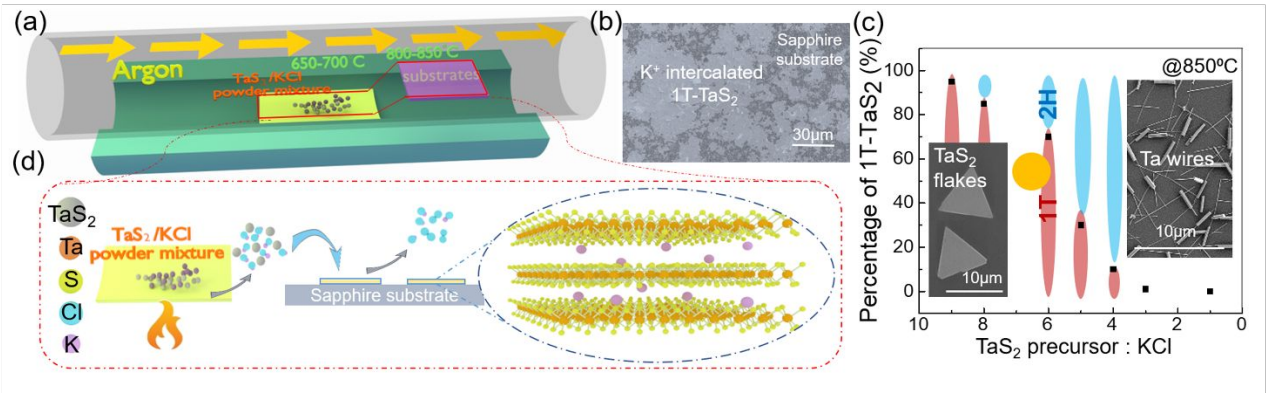

Figure 1: Experiment set-up and intercalation agent impacts on phase change through direct synthesis (a) KCl enhanced TaS_2 lateral growth on sapphire substrate in a quartz tube furnace with two temperature-controlled zones. (b) Morphology of potassium ion incorporated 1T-TaS_2 by SEM. (c) A diagram depicting how the as-synthesized flake phase changes based on precursor: KCl (additive) ratio, with yellow "dot" being chosen in this work for subsequent experiments (d) The diagram demonstrating the proposed KCl-enhanced deposition process

Raman spectroscopy confirms that solid-source CVD grown 1T-TaS_2 exhibits the typical signatures of traditional 1T-TaS_2, with the dominant peak near 78cm^{-1}[35]. However, for K^+ intercalated 1T-TaS_2, the primary Raman peak is split into two sub-peaks. The trend of peak-splitting remains the same when flake thickness increases from 10nm to 30nm (Figure 2a). X-ray photoelectron spectroscopy (XPS) (Figure 2b) indicates significant levels of K present across three different samples with different amount of K^+ incorporation. Normalizing each individual spectrum based on environmental carbon (C) peak intensity-E(C1s) and fixing C1s peak position at 284.8eV, K ion's peak position and intensity can be directly compared. It is found that sample with a higher K 2p binding energy-E (K 2p) shows a slightly lower value of K $2p_{3/2}$ peak position. This observation indicates that the inserted K^+ ions are bonded to S ions, since Cl (from KCl) or O (from substrate-sapphire) are more electronegative than S. The rest of K^+ ion could either be left in KCl or bonded to the surface to help decrease surface energy[36,37]. The small change in the K^+

chemical environment, based on XPS, indicates that the potassium s-electron transfer not a dominating factor in the changing electronic and lattice structures[38]. Comparing Ta 4f peaks between non-intercalated (Figure 2c) and K^+ ion bonded samples (Figure 2d) at room temperature, Ta atoms from non-intercalated samples exhibit more symmetrical peaks than those acquired from samples with K^+ ion incorporation. Peak shoulders of Ta 4f bonds in Figure 2d suggest structural and electronic changes in K-integrated 1T-TaS_2 flakes, since Ta 4f binding energy is particularly sensitive to the local charge density[39]. Moreover, the peak position difference between the Ta_1 and Ta_2 peaks in the Ta $4f_{7/2}$ (ΔCDW)) directly relates to the CDW amplitude[40,41]. Cross section aberration-corrected scanning transmission electron microscopy (STEM) and EDS mapping (Figure 2e, f and Figure S2) indicate K^+ ions exist between individual TaS_2 layers. As marked by the black arrows in Figure 2e and 2f, the TaS_2 interlayer spacing increases after the formation of K^+ interlayer. This enlarged separation could reduce interlayer band dispersions and help open a gap between the chalcogen p and transition-metal d states[42].

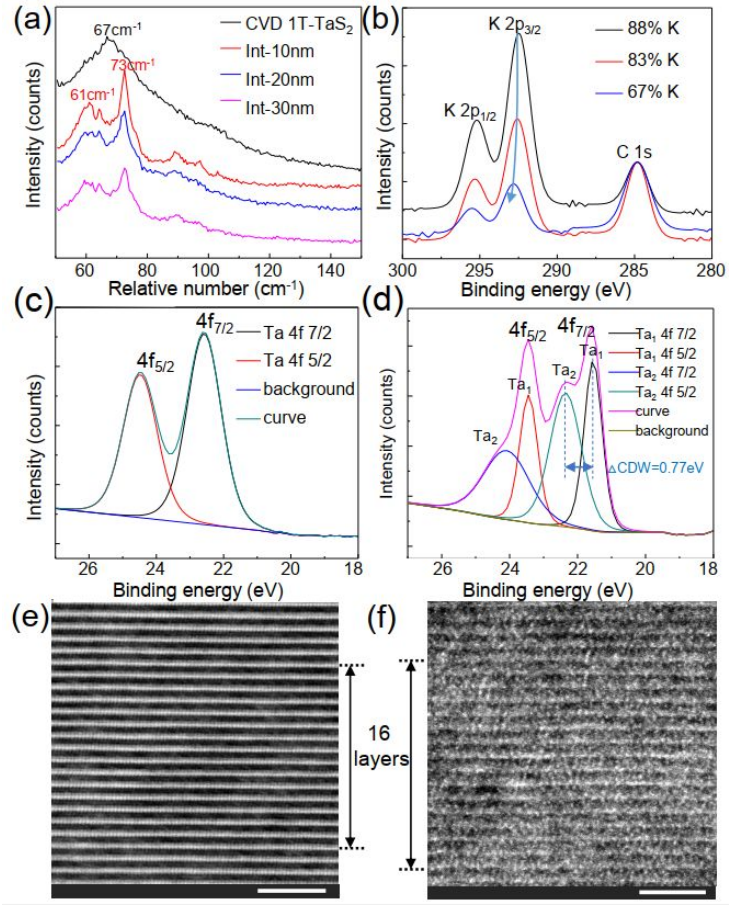

Figure 2: (a) Raman spectroscopy of CDW 1T-TaS_2 flake and three K^+ bonded 1T-TaS_2 with different thicknesses measured at room temperature. (b) Binding energy of K^+ ion within three different samples. Ta4f binding energy of (c) pristine 1T-TaS_2flakes and (d) K^+ bonded 1T-TaS_2 flakes. Cross section TEM imaging of (e) pristine CVD 1T-TaS_2 flakes and of (f) K^+ bonded 1T-TaS_2 flakes at room temperature. Scale bar is 3nm

Temperature dependent Raman spectroscopy indicates that peak features corresponding to the CCDW (near 100cm^{-1})[35] are identified at room temperature (Figure 3a) in K^+ incorporated 1T-TaS_2. These peaks become more distinguished as temperature decreases. Similar groups of phonon

peaks corresponding to Brillouin zone reconstruction are observed[35,43]. Comparing Raman to exfoliated 1T-TaS_2 on sapphire (Figure 3b), we find that one of the CCDW phase-related peaks (61cm^{-1}) red-shifts for the K^+ incorporated samples (up to 63cm^{-1}). This is due to intercalated K^+ induced tensile strain, as reflected in Figure 2f, which shows slightly more distorted layer structure than pristine 1T-TaS_2 layer structure (Figure 2e). Albertini *et al.*[35] reported similar effect theoretically, where positive strains tend to soften vibrational frequencies of 1T-TaS_2 crystal. The same explanation can be applied to the peaks between 70-80cm^{-1}. With K^+ incorporation, the CCDW phase encounters structural distortion, which leads to Raman peak splitting between 70-80 cm^{-1}. However, due to interior strains exerted by exotic ions, the peak splitting is less sharp.

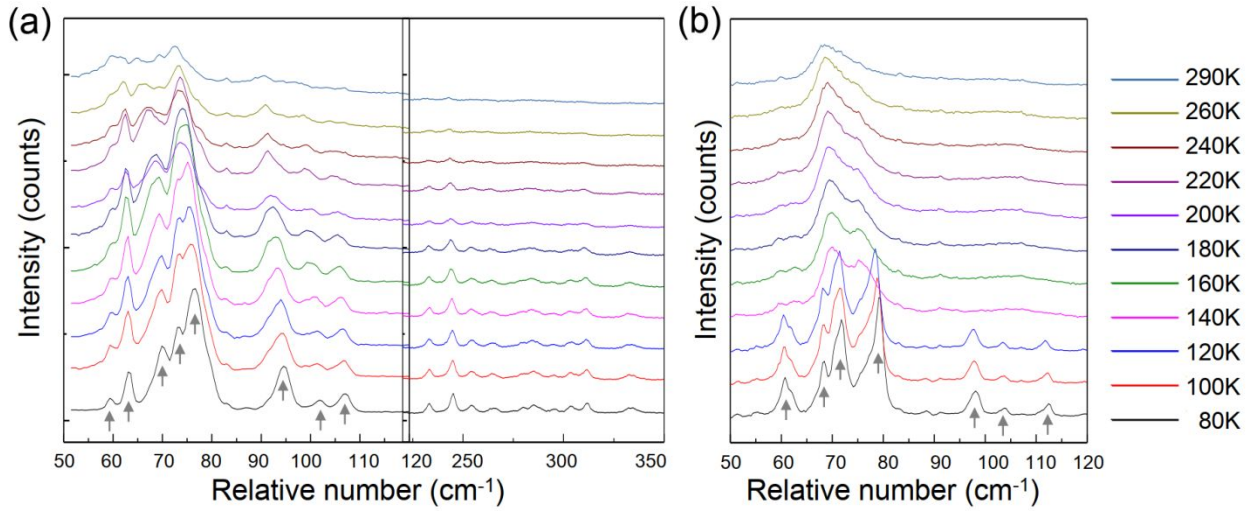

Figure 3: Raman spectra of (a) K^+-incorporated 1T-TaS2 and of (b) exfoliated 1T-TaS_2 flake on sapphire substrate as a function with temperature. Characteristic peaks are marked by grey arrows in both plots. For (a), peak values are: 59cm^{-1}, 63cm^{-1}, 70cm^{-1}, 73cm^{-1}, 76cm^{-1}, 94cm^{-1}, 102cm^{-1} and 107cm^{-1}. For (b), peak values are: 61cm^{-1}, 68cm^{-1}, 72cm^{-1}, 79cm^{-1}, 98cm^{-1}, 104cm^{-1} and 112cm^{-1}.

Temperature-dependent resistance measurements further provide insights on how K^+ interlayers impact 1T-TaS_2 electric properties. Resistance measurement schematic is depicted in Figure 4a. Figure 4b displays the normalized resistivity vs. temperature (ρ-T) for both the pure and K^+ incorporated CVD 1T-TaS_2 films for comparison, where the CCDW-NCCDW phase transition is indicated by an abrupt resistivity change. An enhancement in the phase transition temperature during the heating cycle from 220K in the pristine 1T-TaS_2 to 300K for the K^+ incorporated films as well as a reduction in the ON/OFF ratio for the latter sample are observed. In the cooling cycle, the MIT occurs at approximately the same temperature for both films. Their sheet resistance values are included in Figure S3. Both defects and K^+ induced structural distortion contribute to the increase in the sheet resistance of NCCDW phase of the intercalated 1T-TaS_2. We further investigated K^+ ion position after sample was driven through voltage bias cycling. Cross-section high-angle annular dark-field transmission electron microscopy (HAADF TEM) image (Figure 4c) provides structural and chemical details after electric field has been applied, indicating that there are two distinct regions in the film. The EDS mapping (Figure 4d-g) shows that the K^+ ions primarily lie near the substrate, as opposed to being equally distributed throughout the film (Figure

2f). This indicates that the electric field applied during the ρ-T measurements, which is likely confined to the top layers of the 1T-TaS_2, repels the positively charged K^+ ions to the bottom of the film near the substrate, which leads to the recovery of the pristine 1T-TaS_2 characteristics in the following cooling cycle. Above all, both measurements indicate that the CCDW phase survives to room temperature with the assistance of interlayer K^+ ions.

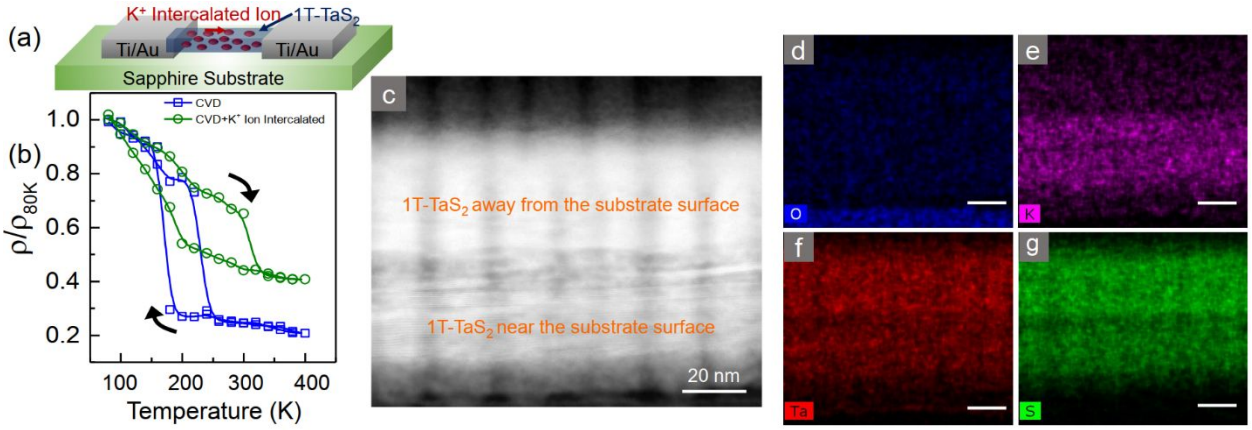

Figure 4: (a) A schematic of the two-terminal device fabricated from the K^+ incorporated 1T-TaS_2 film. (b) Normalized resistivity change for pure solid-source CVD 1T-TaS_2 and K^+ incorporated 1T-TaS_2 demonstrating an increase in the CCDW-NCCDW phase transition to room temperature during heating. (c) Cross-section HAADF-TEM of K^+ incorporated 1T-TaS_2 after an electric field has been applied indicating K+ has been driven out of the channel where the electric field is highest. Elemental EDX mapping of the cross-section TEM in (c): (d) O, (e) K, (f) Ta, (g) S. Scale bar is 20nm

Density functional theory provides evidence that K^+ intercalation impacts chemical bonding in the 1T-TaS_2 that ultimately controls the CDW phase formation. Pristine 1T-TaS_2 (Figure 5a) behaves like a band insulator along the in-plane (ab-plane) direction, whereas it is metallic along the out-of-plane direction (c-plane)[18]. After introducing K^+ ion between TaS_2 layers (Figure 5b), both a and c lattice parameters are increased (Figure 5c), which confirms that the material is under tensile strain as observed from Raman (Figure 3a). The 12% interlayer distance increase observed from cross-section TEM (Figure 2f) correlates well with DFT model with two K atoms intercalated per CDW structure ($K_{interlayer}$/CDW). On the other hand, within each "David" star, two distinct Ta-Ta distances are decreased (Figure 5d), which are labelled as R1 and R2 in the inset of Figure 5d. These two lengths are characteristic of the David star, the smallest unit cell of CCDW structure. The real space charge density distribution of the two structures are calculated in Figure 5e and 5f. With CCDW structure formation, the charges become accumulated within the David star (Figure 5e). Moreover, K^+ helps shift the charge of the outer Ta atoms towards the center and demonstrates a strong charge localization in the center of the cluster (Figure 5f). The energy gain associated with this structure helps illuminate why CCDW phase gets stabilized towards higher temperatures acquired from experiment results (both Raman and transport measurements). However, substituting K for Ta sites in TaS_2 does not improve the stability of the whole structure. The binding energies (BE) of CCDW structures of pure, K-doped, K-interlayered 1T-TaS_2 are summarized in Table 1. Overall, K^+ interlayered TaS_2 enables the lowest BE value in its CCDW structure. This conclusion also helps solidify previous reports where cation doping always shows the inhibition of CCDW structure formation[44,45] while sodium (Na) ion[46], copper (Cu) ion[47],

caesium (Cs) ion[48], lithium (Li) ion[48] or rubidium (Rb) ion[38] *intercalation* of 1T-TaS_2 all lead to an enhancement in CCDW transformation. We note that ion-intercalation-induced CCDW phase could form new superstructures, with some being directly mapped by low energy electron diffraction (LEED)[49–52]. Rb[42] and Cs[48] intercalation yield a novel commensurate $c(2\sqrt{3} \times 4)$rect CDW phase, and Nb intercalation produces a 3×3 or $\sqrt{7} \times \sqrt{7}$ superstructure[46]. To directly understand structural and electronic structural changes brought out by K^+ ion intercalation, future work on low-energy electron or photoelectron diffraction measurements are necessary. Regardless, it can be concluded that cation (particularly, alkali ion) intercalation of 1T-TaS_2 exhibits a great potential of stabilizing CCDW structure towards or above room temperature.

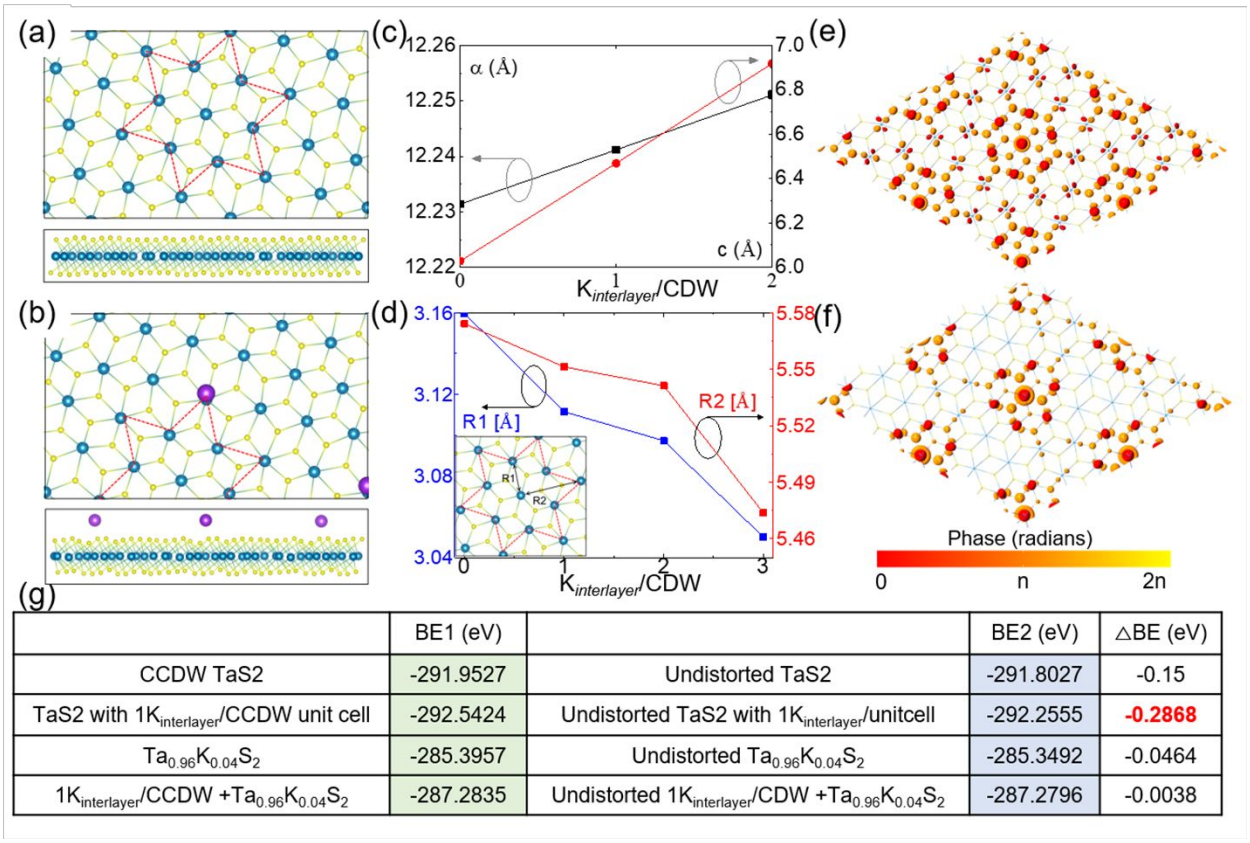

	BE1 (eV)		BE2 (eV)	△BE (eV)
CCDW TaS2	-291.9527	Undistorted TaS2	-291.8027	-0.15
TaS2 with $1K_{interlayer}$/CCDW unit cell	-292.5424	Undistorted TaS2 with $1K_{interlayer}$/unitcell	-292.2555	**-0.2868**
$Ta_{0.96}K_{0.04}S_2$	-285.3957	Undistorted $Ta_{0.96}K_{0.04}S_2$	-285.3492	-0.0464
$1K_{interlayer}$/CCDW +$Ta_{0.96}K_{0.04}S_2$	-287.2835	Undistorted $1K_{interlayer}$/CDW +$Ta_{0.96}K_{0.04}S_2$	-287.2796	-0.0038

Figure 5 DFT calculation of CCDW structure (both top-down view and side-view) of (a) pure 1T-TaS_2 and (b) K^+ incorporated 1T-TaS_2. (c) Change of lattice parameters of a and c of K^+ incorporated 1T-TaS_2 as a function of the amount of $K_{interlayer}$/CDW. (d) Change of CDW characteristic distances (R1 and R2) as a function of K^+ concentration. Real space charge density distribution of (e) pure 1T-TaS_2 and (f) K^+ incorporated 1T-TaS_2. (g) Binding energy (BE) calculations of pure CCDW 1T-TaS2, K-doped CCDW 1T-TaS2 and K^+ incorporated CCDW 1T-TaS2. $1K_{interlayer}$/CCDW unit cell refers to the structure where one K^+ is incorporated with one CCDW structure. $Ta_{0.96}K_{0.04}S_2$ refers to substitutional doping 4% K^+ in 1T-TaS_2 structure. $\Delta BE = BE2 - BE1$

Conclusions

We have presented one route of synthesizing 1T-TaS_2 flakes with K^+ *intercalation* via direct CVD process. By introducing an alkali additive, KCl, the deposition rate and coverage are largely increased and K^+ interlayer growth can be realized in situ. Complementary measurements have shown that interlayer K^+ ions help stabilize the CCDW phase towards room temperature. DFT

calculation revealed that interlayer K^+ helps confine charge distribution within "David star", lowers the chemical binding energy, and thus helps CCDW phase gain stability towards room temperature. Our work can be applied to other 2D CDW materials and help benchmark engineering CDW phase transitions for ultra-low power electronic devices.

Acknowledgements

This work was supported by National Science Foundation Emerging Frontiers in Research and Innovation under the Grant No. EFRI-1433307. RKG wishes to thank Department of Science and Technology, Govt. of India for DST INSPIRE Faculty Grant No. IFA17-ENG206 for financial support.

Reference

1. Novoselov, K. S., Mishchenko, A., Carvalho, A. & Castro Neto, A. H. 2D materials and van der Waals heterostructures. *Science (80-.).* **353**, (2016).
2. Chhowalla, M. *et al.* The chemistry of two-dimensional layered transition metal dichalcogenide nanosheets. *Nat. Chem.* **5**, 263–75 (2013).
3. Bhimanapati, G. R. *et al.* Recent Advances in Two-Dimensional Materials beyond Graphene. *ACS Nano* **9**, 11509–11539 (2015).
4. Liu, H. *et al.* Phosphorene: An unexplored 2D semiconductor with a high hole mobility. *ACS Nano* **8**, 4033–4041 (2014).
5. Neto, A. H. C. Charge Density Wave, Superconductivity , and Anomalous Metallic Behavior in 2D Transition Metal Dichalcogenides. *Phys. Rev. Lett.* **86**, 4382–4385 (2001).
6. Wilson, J. A., Di Salvo, F. J. & Mahajan, S. Charge-Density Waves in Metallic, Layered, Transition-Metal Dichalcogenides. *Phys. Rev. Lett.* **32**, 882–887 (1974).
7. Scruby, C. B., Williams, P. M. & Parry, G. S. The role of charge density waves in structural transformations of 1T TaS2. *Philos. Mag.* **31**, 255–274 (1975).
8. Manzke, R., Buslaps, T., Pfalzgraf, B., Skibowski, M. & Anderson, O. On the phase transitions in 1T-TaS2. *Eur. Lett.* **8**, 195–200 (1989).
9. Sipos, B. *et al.* From Mott state to superconductivity in-1T-TaS2. *Nat. Mater.* **7**, 960–965 (2008).
10. Yu, Y. *et al.* Gate-tunable phase transitions in thin flakes of 1T-TaS2. *Nat. Nanotechnol.* **10**, 270–276 (2015).
11. Di Salvo, F. J., Wilson, J. A., Bagley, B. G. & Waszczak, J. V. Effects of doping on charge-density waves in layer compounds. *Phys. Rev. B* **12**, 2220–2235 (1975).
12. Fukuyama, H. & Yosida, K. Theory of magnetoresistance of 1T-TaS2 and its alloys. *Physica* **105**, 132–135 (1981).
13. Meyer, S. F., Howard, R. E., Stewart, G. R., Acrivos, J. V. & Geballe, T. H. Properties of intercalated 2H-$NbSe_2$, 4Hb-TaS_2, and 1T-TaS_2. *J. Chem. Phys.* **62**, 4411–4419

(1975).

14. Tani, T., Osada, T. & Tanaka, S. The pressure effect on the CDW-transition temperatures in 1 T-TaS 2. *Solid State Commun.* **22**, 269–272 (1977).

15. Zhao, R. *et al.* Tuning Phase Transitions in 1T-TaS 2 via the Substrate. *Nano Lett.* **17**, 3471–3477 (2017).

16. Hollander, M. J. *et al.* Electrically driven reversible insulator-metal phase transition in 1T-TaS2. *Nano Lett.* **15**, 1861–1866 (2015).

17. Vaskivskyi, I. *et al.* Controlling the metal-to-insulator relaxation of the metastable hidden quantum state in 1T-TaS2. *Sci. Adv.* **1**, e1500168 (2015).

18. Grisafe, B., Zhao, R., Ghosh, R. K., Robinson, J. A. & Datta, S. Electrically triggered insulator-to-metal phase transition in two-dimensional (2D) heterostructures. *Appl. Phys. Lett.* **113**, 142101 (2018).

19. Liu, G. *et al.* A charge-density-wave oscillator based on an integrated tantalum disulfide-boron nitride-graphene device operating at room temperature. *Nat. Nanotechnol.* **11**, 845–850 (2016).

20. Yoshida, M., Suzuki, R., Zhang, Y., Nakano, M. & Iwasa, Y. Memristive phase switching in two-dimensional 1T-TaS 2 crystals. *Sci. Adv.* **1**, 1–7 (2015).

21. Liu, Y. *et al.* Superconductivity induced by Se-doping in layered charge-density-wave system 1 T-TaS2−xSex. *Appl. Phys. Lett.* **102**, 192602 (2013).

22. Kim, J.-J., Yamaguchi, W., Hasegawa, T. & Kitazawa, K. Observation ofMott Localization Gap Using Low Temperature Scanning Tunneling Spectroscopy in Commensurate 1T-TaS2. *Phys. Rev. Lett.* **73**, 2103 (1994).

23. Zhao, R., Subramanian, S. & Robinson, J. A. Synthesis, doping and properties of two-dimensional materials. *Int. Soc. Opt. Photonics* **9755**, 97551N (2016).

24. Fu, W. *et al.* Controlled Synthesis of Atomically Thin 1T-TaS 2 for Tunable Charge Density Wave Phase Transitions. *Chem. Mater.* **28**, 7613–7618 (2016).

25. Wang, X. *et al.* Chemical Growth of 1T-TaS 2 Monolayer and Thin Films: Robust Charge Density Wave Transitions and High Bolometric Responsivity. *Adv. Mater.* **30**, 1800074 (2018).

26. Zhao, R. *et al.* Two-dimensional tantalum disulfide : controlling structure and properties via synthesis Two-dimensional tantalum disulfide : controlling structure and properties via synthesis. *2D Mater.* **5**, 025001 (2018).

27. Kaloyeros, A. E. *et al.* Tantalum Nitride Films Grown by Inorganic Low Temperature Thermal Chemical Vapor Deposition Diffusion Barrier Properties in Copper Metallization. *J. Electrochem. Soc.* **146**, 170–176 (1999).

28. Wiedmann, M. K., Heeg, M. J. & Winter, C. H. Volatility and high thermal stability in tantalum complexes containing imido, amidinate, and halide or dialkylamide ligands. *Inorg. Chem.* **48**, 5382–5391 (2009).

29. Kim, H., Ovchinnikov, D., Deiana, D., Unuchek, D. & Kis, A. Suppressing Nucleation in Metal–Organic Chemical Vapor Deposition of MoS2 Monolayers by Alkali Metal Halides. *Nano Lett.* **17**, 5056–5063 (2017).

30. Kang, K. *et al.* High-mobility three-atom-thick semiconducting films with wafer-scale homogeneity. *Nature* **520**, 656–660 (2015).

31. Jellinek, F. The system tantalum-sulfur. *J. Less Common Met.* **4**, 9–15 (1962).

32. *NIST Chemistry WebBook, NIST Standard Reference Database Number 69*. (National Institute of Standards and Technology, Gaithersburg MD, 20899, 2018). doi:https://doi.org/10.18434/T4D303

33. Mattheiss, L. F. Band Structures of Transition-Metal-Dichalcogenide Layer Compounds. *Phys. Rev. B* **8**, 3719 (1973).

34. Beinik, I., Barth, C., Hanbücken, M. & Masson, L. KCl ultra-thin films with polar and non-polar surfaces grown on Si(111)7 × 7. *Sci. Rep.* **5**, 8223 (2015).

35. Albertini, O. R. *et al.* Zone-center phonons of bulk, few-layer, and monolayer 1T-TaS2: Detection of commensurate charge density wave phase through Raman scattering. *Phys. Rev. B* **93**, 1–7 (2016).

36. Liu, B. & Zeng, H. C. Salt-Assisted Deposition of SnO2 on a-MoO3 Nanorods and Fabrication of Polycrystalline SnO2 Nanotubes. *J. Phys. Chem. B* **108**, 5867–5874 (2004).

37. Zhou, J. *et al.* Salt-template-assisted synthesis of robust 3D honeycomb-like structured MoS2and its application as a lithium-ion battery anode. *J. Mater. Chem. A* **4**, 8734–8741 (2016).

38. Rossnagel, K. Suppression and emergence of charge-density waves at the surfaces of layered 1T- TiSe2 and 1T-TaS2 by in situ Rb deposition. *New J. Phys.* **12**, 125018 (2010).

39. Hellmann, S. *et al.* Ultrafast Melting of a Charge-Density Wave in the Mott Insulator 1 T - TaS 2. *Phys. Rev. Lett.* **105**, 187401 (2010).

40. Hughes, H. P. & Pollak, R. A. Charge density waves in layered metals observed by X-ray photoemission. *Philos. Mag.* **34**, 1025–1046 (1976).

41. Hughes, H. P. & Scarfe, J. A. Site Specific Photohole Screening in a Charge Density Wave. *Phys. Rev. Lett.* **74**, 3069–3072 (1995).

42. Rahn, D. J. *et al.* Laterally confined metal-to-insulator and quasi-two-dimensional-to-two-dimensional transition by focused Rb intercalation of 1T-TaS2. *Phys. Rev. B* **84**, 233105 (2011).

43. He, R. *et al.* Distinct surface and bulk charge density waves in ultrathin 1T-TaS2. *Phys. Rev. B* **94**, 201108 (2016).

44. Li, L. J. *et al.* Fe-doping-induced superconductivity in the charge-density-wave system 1T-TaS2. *EPL (Europhysics Lett.* **97**, 67005 (2012).

45. Fujimoto, H. & Ozaki, H. EFFECTS OF Hf AND W DOPING ON THE

COMMENSURATE CHARGE DENSITY WAVES IN IT-TaS2. *Solid State Commun.* **49**, 1117–1119 (1984).

46. Pettenkofer, C. & Jaegermann, W. Charge-density-wave transformation induced by Na intercalation into 1T-TaS2. *Phys. Rev. B* **50**, 8816 (1994).

47. Pettenkofer, C., Jaegermann, W. & Parkinson, B. A. Copper intercalation in 1T-TaS2. *Surf. Sci.* **251**–**252**, 583–586 (1991).

48. Crawack, H. J. & Pettenkofer, C. Calculation and XPS measurements of the Ta4f CDW splitting in Cu, Cs and Li intercalation phases of 1T-TaX2(X = S, Se). *Solid State Commun.* **118**, 325–332 (2001).

49. Vogelgesang, S. *et al.* Phase ordering of charge density waves traced by ultrafast low-energy electron diffraction. *Nat. Phys.* **14**, 184–190 (2018).

50. Gulde, M. *et al.* Ultrafast low-energy electron diffraction in transmission resolves polymer/graphene superstructure dynamics. *Science (80-.).* **345**, 200–204 (2014).

51. Becker, R. S., Higashi, G. S. & Golovchenko, J. A. Low-Energy Electron Diffraction during Pulsed Laser Annealing: A Time-Resolved Surface Structural Study. *Phys. Rev. Lett.* **52**, 307–310 (1984).

52. Müller, M., Paarmann, A. & Ernstorfer, R. Femtosecond electrons probing currents and atomic structure in nanomaterials. *Nat. Commun.* **5**, 5292 (2014).